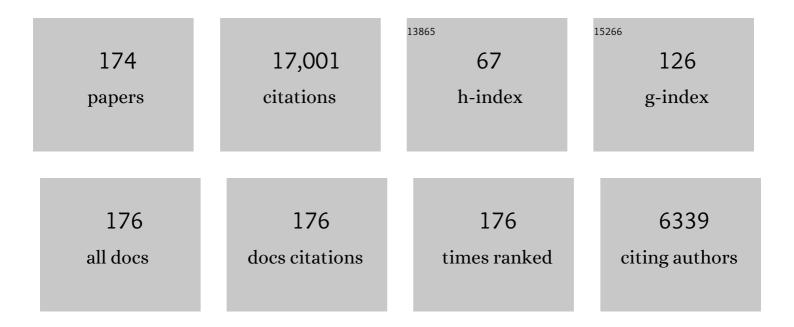
Gregory A Neumann

List of Publications by Year in descending order

Source: https://exaly.com/author-pdf/7489555/publications.pdf Version: 2024-02-01



#	Article	IF	CITATIONS
1	Geodetic investigations of the mission concept MAGIC to reveal Callisto's internal structure. Acta Astronautica, 2022, 195, 68-76.	3.2	5
2	Improved LOLA elevation maps for south pole landing sites: Error estimates and their impact on illumination conditions. Planetary and Space Science, 2021, 203, 105119.	1.7	48
3	Deriving Mercury Geodetic Parameters With Altimetric Crossovers From the Mercury Laser Altimeter (MLA). Journal of Geophysical Research E: Planets, 2021, 126, e2020JE006683.	3.6	9
4	Degassing of volcanic extrusives on Mercury: Potential contributions to transient atmospheres and buried polar deposits. Earth and Planetary Science Letters, 2021, 564, 116907.	4.4	6
5	Rotational states and shapes of Ryugu and Bennu: Implications for interior structure and strength. Planetary and Space Science, 2021, 204, 105268.	1.7	15
6	Analyzing the ages of south polar craters on the Moon: Implications for the sources and evolution of surface water ice Icarus, 2020, 336, 113455.	2.5	53
7	Highâ€Resolution Gravity Field Models from GRAIL Data and Implications for Models of the Density Structure of the Moon's Crust. Journal of Geophysical Research E: Planets, 2020, 125, e2019JE006086.	3.6	38
8	Digital terrain mapping by the OSIRIS-REx mission. Planetary and Space Science, 2020, 180, 104764.	1.7	81
9	Hemispherical differences in the shape and topography of asteroid (101955) Bennu. Science Advances, 2020, 6, .	10.3	57
10	Temperatureâ€Dependent Changes in the Normal Albedo of the Lunar Surface at 1,064Ânm. Journal of Geophysical Research E: Planets, 2020, 125, e2019JE006338.	3.6	4
11	Assessing the Roughness Properties of Circumpolar Lunar Craters: Implications for the Timing of Waterâ€kce Delivery to the Moon. Geophysical Research Letters, 2020, 47, e2020GL087782.	4.0	13
12	First two-way laser ranging to a lunar orbiter: infrared observations from the Grasse station to LRO's retro-reflector array. Earth, Planets and Space, 2020, 72, .	2.5	10
13	Searching for Lunar Horizon Glow With the Lunar Orbiter Laser Altimeter. Journal of Geophysical Research E: Planets, 2019, 124, 2728-2744.	3.6	6
14	The thickness of radar-bright deposits in Mercury's northern hemisphere from individual Mercury Laser Altimeter tracks. Icarus, 2019, 323, 40-45.	2.5	10
15	Age constraints of Mercury's polar deposits suggest recent delivery of ice. Earth and Planetary Science Letters, 2019, 520, 26-33.	4.4	19
16	GRAIL-identified gravity anomalies in Oceanus Procellarum: Insight into subsurface impact and magmatic structures on the Moon. Icarus, 2019, 331, 192-208.	2.5	20
17	Geodetic Evidence That Mercury Has A Solid Inner Core. Geophysical Research Letters, 2019, 46, 3625-3633.	4.0	80
18	Shape of (101955) Bennu indicative of a rubble pile with internal stiffness. Nature Geoscience, 2019, 12, 247-252.	12.9	179

#	Article	IF	CITATIONS
19	Trilogy, a planetary geodesy mission concept for measuring the expansion of the solar system. Planetary and Space Science, 2018, 153, 127-133.	1.7	8
20	Solar system expansion and strong equivalence principle as seen by the NASA MESSENGER mission. Nature Communications, 2018, 9, 289.	12.8	81
21	Constraining the thickness of polar ice deposits on Mercury using the Mercury Laser Altimeter and small craters in permanently shadowed regions. Icarus, 2018, 305, 139-148.	2.5	17
22	Ring faults and ring dikes around the Orientale basin on the Moon. Icarus, 2018, 310, 1-20.	2.5	31
23	Orbit determination of the Lunar Reconnaissance Orbiter: Status after seven years. Planetary and Space Science, 2018, 162, 2-19.	1.7	39
24	Illumination conditions at the lunar poles: Implications for future exploration. Planetary and Space Science, 2018, 162, 170-178.	1.7	53
25	Mercury's Crust and Lithosphere: Structure and Mechanics. , 2018, , 52-84.		9
26	Mercury's Polar Deposits. , 2018, , 346-370.		9
27	In-flight characterization of the lunar orbiter laser altimeter instrument pointing and far-field pattern. Applied Optics, 2018, 57, 7702.	1.8	6
28	lce in Micro Cold Traps on Mercury: Implications for Age and Origin. Journal of Geophysical Research E: Planets, 2018, 123, 2178-2191.	3.6	19
29	Observational constraints on the identification of shallow lunar magmatism: Insights from floor-fractured craters. Icarus, 2017, 283, 224-231.	2.5	23
30	Evidence for surface water ice in the lunar polar regions using reflectance measurements from the Lunar Orbiter Laser Altimeter and temperature measurements from the Diviner Lunar Radiometer Experiment. Icarus, 2017, 292, 74-85.	2.5	119
31	GRAIL gravity observations of the transition from complex crater to peak-ring basin on the Moon: Implications for crustal structure and impact basin formation. Icarus, 2017, 292, 54-73.	2.5	19
32	New evidence for surface water ice in smallâ€scale cold traps and in three large craters at the north polar region of Mercury from the Mercury Laser Altimeter. Geophysical Research Letters, 2017, 44, 9233-9241.	4.0	37
33	Evidence for a low bulk crustal density for Mars from gravity and topography. Geophysical Research Letters, 2017, 44, 7686-7694.	4.0	82
34	Analysis of one-way laser ranging data to LRO, time transfer and clock characterization. Icarus, 2017, 283, 38-54.	2.5	12
35	Low-amplitude topographic features and textures on the Moon: Initial results from detrended Lunar Orbiter Laser Altimeter (LOLA) topography. Icarus, 2017, 283, 138-145.	2.5	13
36	Summary of the results from the lunar orbiter laser altimeter after seven years in lunar orbit. Icarus, 2017, 283, 70-91.	2.5	116

#	Article	IF	CITATIONS
37	The laser ranging experiment of the Lunar Reconnaissance Orbiter: Five years of operations and data analysis. Icarus, 2017, 283, 55-69.	2.5	23
38	ICESAT/GLAS Altimetry Measurements: Received Signal Dynamic Range and Saturation Correction. IEEE Transactions on Geoscience and Remote Sensing, 2017, 55, 5440-5454.	6.3	22
39	Comparison of areas in shadow from imaging and altimetry in the north polar region of Mercury and implications for polar ice deposits. Icarus, 2016, 280, 158-171.	2.5	40
40	Demonstration of orbit determination for the Lunar Reconnaissance Orbiter using one-way laser ranging data. Planetary and Space Science, 2016, 129, 32-46.	1.7	11
41	Subsurface morphology and scaling of lunar impact basins. Journal of Geophysical Research E: Planets, 2016, 121, 1695-1712.	3.6	37
42	Gravity field of the Orientale basin from the Gravity Recovery and Interior Laboratory Mission. Science, 2016, 354, 438-441.	12.6	38
43	Lunar phase function at 1064Ânm from Lunar Orbiter Laser Altimeter passive and active radiometry. Icarus, 2016, 273, 96-113.	2.5	19
44	Seasonal and static gravity field of Mars from MGS, Mars Odyssey and MRO radio science. Icarus, 2016, 272, 228-245.	2.5	172
45	Improved calibration of reflectance data from the LRO Lunar Orbiter Laser Altimeter (LOLA) and implications for space weathering. Icarus, 2016, 273, 315-328.	2.5	34
46	A new lunar digital elevation model from the Lunar Orbiter Laser Altimeter and SELENE Terrain Camera. Icarus, 2016, 273, 346-355.	2.5	326
47	Baseline Design and Performance Analysis of Laser Altimeter for Korean Lunar Orbiter. Journal of Astronomy and Space Sciences, 2016, 33, 211-219.	1.0	3
48	The lowâ€degree shape of Mercury. Geophysical Research Letters, 2015, 42, 6951-6958.	4.0	36
49	The fractured Moon: Production and saturation of porosity in the lunar highlands from impact cratering. Geophysical Research Letters, 2015, 42, 6939-6944.	4.0	63
50	First <scp>MESSENGER</scp> orbital observations of Mercury's librations. Geophysical Research Letters, 2015, 42, 7881-7889.	4.0	44
51	Calibration of the Mercury Laser Altimeter on the MESSENGER Spacecraft. IEEE Transactions on Geoscience and Remote Sensing, 2015, 53, 2860-2874.	6.3	22
52	Lunar impact basins revealed by Gravity Recovery and Interior Laboratory measurements. Science Advances, 2015, 1, e1500852.	10.3	173
53	Deep-seated thrust faults bound the Mare Crisium lunar mascon. Earth and Planetary Science Letters, 2015, 427, 183-190.	4.4	39
54	Simulated recovery of Europa's global shape and tidal Love numbers from altimetry and radio tracking during a dedicated flyby tour. Geophysical Research Letters, 2015, 42, 3166-3173.	4.0	17

#	Article	IF	CITATIONS
55	Low-altitude magnetic field measurements by MESSENGER reveal Mercury's ancient crustal field. Science, 2015, 348, 892-895.	12.6	89
56	The age of lunar south circumpolar craters Haworth, Shoemaker, Faustini, and Shackleton: Implications for regional geology, surface processes, and volatile sequestration. Icarus, 2015, 255, 70-77.	2.5	36
57	Stratigraphy of the Caloris basin, Mercury: Implications for volcanic history and basin impact melt. Icarus, 2015, 250, 413-429.	2.5	49
58	The global albedo of the Moon at 1064 nm from LOLA. Journal of Geophysical Research E: Planets, 2014, 119, 1665-1679.	3.6	96
59	Kilometerâ€scale topographic roughness of Mercury: Correlation with geologic features and units. Geophysical Research Letters, 2014, 41, 8245-8251.	4.0	39
60	Detection of the lunar body tide by the Lunar Orbiter Laser Altimeter. Geophysical Research Letters, 2014, 41, 2282-2288.	4.0	45
61	In-flight performance of the Mercury Laser Altimeter laser transmitter. Proceedings of SPIE, 2014, , .	0.8	0
62	Images of surface volatiles in Mercury's polar craters acquired by the MESSENGER spacecraft. Geology, 2014, 42, 1051-1054.	4.4	67
63	Illumination conditions at the lunar south pole using high resolution Digital Terrain Models from LOLA. Icarus, 2014, 243, 78-90.	2.5	65
64	Structure and evolution of the lunar Procellarum region as revealed by GRAIL gravity data. Nature, 2014, 514, 68-71.	27.8	85
65	The formation of lunar mascon basins from impact to contemporary form. Journal of Geophysical Research E: Planets, 2014, 119, 2378-2397.	3.6	57
66	The location of Airyâ€0, the Mars prime meridian reference, from stereo photogrammetric processing of THEMIS IR imaging and digital elevation data. Journal of Geophysical Research E: Planets, 2014, 119, 2471-2486.	3.6	6
67	Global inventory and characterization of pyroclastic deposits on Mercury: New insights into pyroclastic activity from MESSENGER orbital data. Journal of Geophysical Research E: Planets, 2014, 119, 635-658.	3.6	79
68	The gravity field, orientation, and ephemeris of Mercury from MESSENGER observations after three years in orbit. Journal of Geophysical Research E: Planets, 2014, 119, 2417-2436.	3.6	110
69	Lunar interior properties from the GRAIL mission. Journal of Geophysical Research E: Planets, 2014, 119, 1546-1578.	3.6	185
70	Highâ€resolution local gravity model of the south pole of the Moon from GRAIL extended mission data. Geophysical Research Letters, 2014, 41, 3367-3374.	4.0	12
71	Global characteristics of porosity and density stratification within the lunar crust from GRAIL gravity and Lunar Orbiter Laser Altimeter topography data. Geophysical Research Letters, 2014, 41, 1882-1889.	4.0	38
72	GRGM900C: A degree 900 lunar gravity model from GRAIL primary and extended mission data. Geophysical Research Letters, 2014, 41, 3382-3389.	4.0	152

#	Article	IF	CITATIONS
73	Co-registration of laser altimeter tracks with digital terrain models and applications in planetary science. Planetary and Space Science, 2013, 89, 111-117.	1.7	32
74	The lunar moho and the internal structure of the Moon: A geophysical perspective. Tectonophysics, 2013, 609, 331-352.	2.2	59
75	Asymmetric Distribution of Lunar Impact Basins Caused by Variations in Target Properties. Science, 2013, 342, 724-726.	12.6	103
76	Ancient Igneous Intrusions and Early Expansion of the Moon Revealed by GRAIL Gravity Gradiometry. Science, 2013, 339, 675-678.	12.6	177
77	Gravity Field of the Moon from the Gravity Recovery and Interior Laboratory (GRAIL) Mission. Science, 2013, 339, 668-671.	12.6	389
78	The Crust of the Moon as Seen by GRAIL. Science, 2013, 339, 671-675.	12.6	726
79	Bright and Dark Polar Deposits on Mercury: Evidence for Surface Volatiles. Science, 2013, 339, 296-300.	12.6	197
80	Thermal Stability of Volatiles in the North Polar Region of Mercury. Science, 2013, 339, 300-303.	12.6	119
81	Lunar topographic roughness maps from Lunar Orbiter Laser Altimeter (LOLA) data: Scale dependence and correlation with geologic features and units. Icarus, 2013, 226, 52-66.	2.5	90
82	Simultaneous laser ranging and communication from an Earth-based satellite laser ranging station to the Lunar Reconnaissance Orbiter in lunar orbit. , 2013, , .		6
83	The Origin of Lunar Mascon Basins. Science, 2013, 340, 1552-1555.	12.6	174
84	Space Lidar Developed at the NASA Goddard Space Flight Center—The First 20 Years. IEEE Journal of Selected Topics in Applied Earth Observations and Remote Sensing, 2013, 6, 1660-1675.	4.9	25
85	Free space laser communication experiments from Earth to the Lunar Reconnaissance Orbiter in lunar orbit. Optics Express, 2013, 21, 1865.	3.4	63
86	High‒degree gravity models from GRAIL primary mission data. Journal of Geophysical Research E: Planets, 2013, 118, 1676-1698.	3.6	114
87	Investigating the origin of candidate lava channels on Mercury with MESSENGER data: Theory and observations. Journal of Geophysical Research E: Planets, 2013, 118, 471-486.	3.6	38
88	Gravity Field and Internal Structure of Mercury from MESSENGER. Science, 2012, 336, 214-217.	12.6	305
89	Constraints on the volatile distribution within Shackleton crater at the lunar south pole. Nature, 2012, 486, 378-381.	27.8	159
90	Instrument design and in orbit performance of planetary lidars developed at NASA GSFC. , 2012, , .		0

Instrument design and in orbit performance of planetary lidars developed at NASA GSFC. , 2012, , . 90

#	Article	IF	CITATIONS
91	Topography of the Northern Hemisphere of Mercury from MESSENGER Laser Altimetry. Science, 2012, 336, 217-220.	12.6	223
92	Characterization of the morphometry of impact craters hosting polar deposits in Mercury's north polar region. Journal of Geophysical Research, 2012, 117, .	3.3	17
93	Testing lunar permanently shadowed regions for water ice: LEND results from LRO. Journal of Geophysical Research, 2012, 117, .	3.3	49
94	Lunar impact basins: Stratigraphy, sequence and ages from superposed impact crater populations measured from Lunar Orbiter Laser Altimeter (LOLA) data. Journal of Geophysical Research, 2012, 117, .	3.3	114
95	The transition from complex craters to multiâ€ring basins on the Moon: Quantitative geometric properties from Lunar Reconnaissance Orbiter Lunar Orbiter Laser Altimeter (LOLA) data. Journal of Geophysical Research, 2012, 117, .	3.3	40
96	Lunar floorâ€fractured craters: Classification, distribution, origin and implications for magmatism and shallow crustal structure. Journal of Geophysical Research, 2012, 117, .	3.3	99
97	Large impact basins on Mercury: Global distribution, characteristics, and modification history from MESSENGER orbital data. Journal of Geophysical Research, 2012, 117, .	3.3	68
98	Global maps of lunar neutron fluxes from the LEND instrument. Journal of Geophysical Research, 2012, 117, .	3.3	35
99	Locating the LCROSS Impact Craters. Space Science Reviews, 2012, 167, 71-92.	8.1	11
100	The morphology of craters on Mercury: Results from MESSENGER flybys. Icarus, 2012, 219, 414-427.	2.5	53
101	Orbit determination of the Lunar Reconnaissance Orbiter. Journal of Geodesy, 2012, 86, 193-207.	3.6	117
102	Global surface slopes and roughness of the Moon from the Lunar Orbiter Laser Altimeter. Journal of Geophysical Research, 2011, 116, .	3.3	149
103	Thickness of proximal ejecta from the Orientale Basin from Lunar Orbiter Laser Altimeter (LOLA) data: Implications for multi-ring basin formation. Geophysical Research Letters, 2011, 38, n/a-n/a.	4.0	68
104	The transition from complex crater to peak-ring basin on the Moon: New observations from the Lunar Orbiter Laser Altimeter (LOLA) instrument. Icarus, 2011, 214, 377-393.	2.5	74
105	Report of the IAU Working Group on Cartographic Coordinates and Rotational Elements: 2009. Celestial Mechanics and Dynamical Astronomy, 2011, 109, 101-135.	1.4	305
106	Illumination conditions of the lunar polar regions using LOLA topography. Icarus, 2011, 211, 1066-1081.	2.5	218
107	Clobal Distribution of Large Lunar Craters: Implications for Resurfacing and Impactor Populations. Science, 2010, 329, 1504-1507.	12.6	210
108	Geodetic constraints from multi-beam laser altimeter crossovers. Journal of Geodesy, 2010, 84, 343-354.	3.6	25

#	Article	IF	CITATIONS
109	The Lunar Reconnaissance Orbiter Laser Ranging Investigation. Space Science Reviews, 2010, 150, 63-80.	8.1	91
110	The Lunar Orbiter Laser Altimeter Investigation onÂtheÂLunar Reconnaissance Orbiter Mission. Space Science Reviews, 2010, 150, 209-241.	8.1	394
111	Accommodation of lithospheric shortening on Mercury from altimetric profiles of ridges and lobate scarps measured during MESSENGER flybys 1 and 2. Icarus, 2010, 209, 247-255.	2.5	29
112	The equatorial shape and gravity field of Mercury from MESSENGER flybys 1 and 2. Icarus, 2010, 209, 88-100.	2.5	43
113	Initial observations from the Lunar Orbiter Laser Altimeter (LOLA). Geophysical Research Letters, 2010, 37, .	4.0	356
114	Hydrogen Mapping of the Lunar South Pole Using the LRO Neutron Detector Experiment LEND. Science, 2010, 330, 483-486.	12.6	265
115	Seeing the Missing Half. Science, 2009, 323, 885-887.	12.6	5
116	Mercury's internal magnetic field: Constraints on large- and small-scale fields of crustal origin. Earth and Planetary Science Letters, 2009, 285, 340-346.	4.4	22
117	Time variations of Mars' gravitational field and seasonal changes in the masses of the polar ice caps. Journal of Geophysical Research, 2009, 114, .	3.3	25
118	The Lunar Orbiter Laser Altimeter Investigation onÂtheÂLunar Reconnaissance Orbiter Mission. , 2009, , 209-241.		10
119	The Lunar Reconnaissance Orbiter Laser Ranging Investigation. , 2009, , 63-80.		4
120	Laser Altimeter Measurements from MESSENGERâ \in Ms Recent Mercury Flybys. , 2009, , .		1
121	Interannual and seasonal behavior of Martian residual ice-cap albedo. Planetary and Space Science, 2008, 56, 194-211.	1.7	33
122	Laser Altimeter Observations from MESSENGER's First Mercury Flyby. Science, 2008, 321, 77-79.	12.6	44
123	LASER RANGING FOR GRAVITATIONAL, LUNAR AND PLANETARY SCIENCE. International Journal of Modern Physics D, 2007, 16, 2151-2164.	2.1	21
124	Diurnal variation and radiative influence of Martian water ice clouds. Geophysical Research Letters, 2007, 34, .	4.0	82
125	The Geophysics of Mercury: Current Status and Anticipated Insights from the MESSENGER Mission. Space Science Reviews, 2007, 131, 105-132.	8.1	27
126	The Mercury Laser Altimeter Instrument for the MESSENGER Mission. Space Science Reviews, 2007, 131, 451-479.	8.1	231

ARTICLE IF CITATIONS Report of the IAU/IAG Working Group on cartographic coordinates and rotational elements: 2006. 1.4 Celestial Mechanics and Dynamical Astronomy, 2007, 98, 155-180. The Mercury Laser Altimeter Instrument for the MESSENGER Mission., 2007,, 451-479. 128 8 The Geophysics of Mercury: Current Status and Anticipated Insights from the MESSENGER Mission., 129 2007, , 105-132. Mars 1064 nm spectral radiance measurements determined from the receiver noise response of the 130 2.1 20 Mars Orbiter Laser Altimeter. Applied Optics, 2006, 45, 3960. Two-Way Laser Link over Interplanetary Distance. Science, 2006, 311, 53-53. 12.6 Photogrammetric Analysis of the Mars Global Surveyor Mapping Data. Photogrammetric Engineering 132 0.6 20 and Remote Sensing, 2005, 71, 97-108. New Perspectives on Ancient Mars. Science, 2005, 307, 1214-1220. 12.6 265 Improved estimate of tidal dissipation within Mars from MOLA observations of the shadow of Phobos. 134 3.3 94 Journal of Geophysical Research, 2005, 110, . Depth, distribution, and density of CO2deposition on Mars. Journal of Geophysical Research, 2004, 109, 3.3 136 Crustal structure of Mars from gravity and topography. Journal of Geophysical Research, 2004, 109, . 3.3 360 Correction to $\hat{a} \in \mathbb{C}$ Localized gravity/topography admittance and correlation spectra on Mars: 3.3 Implications for regional and global evolutiona€. Journal of Geophysical Research, 2004, 109, . Two Mars years of clouds detected by the Mars Orbiter Laser Altimeter. Journal of Geophysical 138 3.3 58 Research, 2003, 108, . Mars Orbiter Laser Altimeter pulse width measurements and footprint-scale roughness. Geophysical 4.0 89 Research Letters, 2003, 30, . Analysis of MOLA data for the Mars Exploration Rover landing sites. Journal of Geophysical Research, 140 3.3 25 2003, 108, . Localized gravity/topography admittance and correlation spectra on Mars: Implications for regional 3.3 243 and global evolution. Journal of Geophysical Research, 2002, 107, 19-1-19-25. Small-Scale Topography of 433 Eros from Laser Altimetry and Imaging. Icarus, 2002, 155, 51-74. 142 2.5 66 Comparison of Viking Lander Descent Data and MOLA Topography Reveals Kilometer-Scale Offset in 2.5 Mars Atmosphere Profiles. Icarus, 2002, 159, 259-261. Extension and uplift at Alba Patera, Mars: Insights from MOLA observations and loading models. 144 3.3 27 Journal of Geophysical Research, 2001, 106, 23769-23809.

#	Article	IF	CITATIONS
145	Mars Orbiter Laser Altimeter: Experiment summary after the first year of global mapping of Mars. Journal of Geophysical Research, 2001, 106, 23689-23722.	3.3	1,344
146	Crossover analysis of Mars Orbiter Laser Altimeter data. Journal of Geophysical Research, 2001, 106, 23753-23768.	3.3	145
147	An improved solution of the gravity field of Mars (GMM-2B) from Mars Global Surveyor. Journal of Geophysical Research, 2001, 106, 23359-23376.	3.3	227
148	Enigmatic northern plains of Mars. Nature, 2001, 410, 651-651.	27.8	36
149	Laser Altimetry of Small-Scale Features on 433 Eros from NEAR-Shoemaker. Science, 2001, 292, 488-491.	12.6	38
150	Seasonal Variations of Snow Depth on Mars. Science, 2001, 294, 2141-2146.	12.6	212
151	Internal Structure and Early Thermal Evolution of Mars from Mars Global Surveyor Topography and Gravity. Science, 2000, 287, 1788-1793.	12.6	518
152	The Shape of 433 Eros from the NEAR-Shoemaker Laser Rangefinder. Science, 2000, 289, 2097-2101.	12.6	171
153	The Global Topography of Mars and Implications for Surface Evolution. Science, 1999, 284, 1495-1503.	12.6	826
154	The use of laser altimetry in the orbit and attitude determination of Mars Global Surveyor. Geophysical Research Letters, 1999, 26, 1191-1194.	4.0	57
155	Mars: Northern hemisphere slopes and slope distributions. Geophysical Research Letters, 1998, 25, 4413-4416.	4.0	48
156	Shape of the northern hemisphere of Mars from the Mars Orbiter Laser Altimeter (MOLA). Geophysical Research Letters, 1998, 25, 4393-4396.	4.0	23
157	Observations of the North Polar Region of Mars from the Mars Orbiter Laser Altimeter. , 1998, 282, 2053-2060.		231
158	A 70th degree lunar gravity model (GLGM-2) from Clementine and other tracking data. Journal of Geophysical Research, 1997, 102, 16339-16359.	3.3	125
159	Topography of the Moon from the Clementine lidar. Journal of Geophysical Research, 1997, 102, 1591-1611.	3.3	246
160	Electromagnetic core-mantle coupling and paleomagnetic reversal paths. Geophysical Research Letters, 1996, 23, 2705-2708.	4.0	14
161	The lunar crust: Global structure and signature of major basins. Journal of Geophysical Research, 1996, 101, 16841-16863.	3.3	206
162	High Degree and Order Spherical Harmonic Models for the Moon From Clementine and Historic S-Band Data. International Association of Geodesy Symposia, 1996, , 176-185.	0.4	1

#	Article	IF	CITATIONS
163	High resolution statistical estimation of seafloor morphology: Oblique and orthogonal fabric on the flanks of the Mid-Atlantic Ridge, 34�?35.5� S. Marine Geophysical Researches, 1995, 17, 221-250.	1.2	33
164	The Shape and Internal Structure of the Moon from the Clementine Mission. Science, 1994, 266, 1839-1843.	12.6	349
165	Mantle control of a dynamically evolving spreading center: Mid-Atlantic Ridge 31–34°S. Earth and Planetary Science Letters, 1994, 121, 451-468.	4.4	70
166	Comparison of marine gravity from shipboard and highâ€density satellite altimetry along the Midâ€Atlantic Ridge, 30.5°–35.5°S. Geophysical Research Letters, 1993, 20, 1639-1642.	4.0	47
167	The paradox of the axial profile: Isostatic compensation along the axis of the Midâ€Atlantic Ridge?. Journal of Geophysical Research, 1993, 98, 17891-17910.	3.3	106
168	The Rio Grande rift: new electromagnetic constraints on the Socorro magma body. Physics of the Earth and Planetary Interiors, 1991, 66, 101-117.	1.9	15
169	Magnetic variations in the reconnaissance of sedimentary basins: Field procedure and generalized inversion of shortâ€period data from the Rio Grande rift. Geophysics, 1990, 55, 1567-1576.	2.6	1
170	A high-density remote reference magnetic variation profile in the Pacific northwest of North America. Physics of the Earth and Planetary Interiors, 1989, 53, 305-319.	1.9	7
171	Evidence for multiple boundary faults beneath the northwest moat of Long Valley Caldera: Magnetotelluric results. Geophysical Research Letters, 1988, 15, 1437-1440.	4.0	6
172	The regional subsurface structure of Long Valley (California) caldera fill from gravity and magnetotelluric data. Bulletin of the Geological Society of America, 1988, 100, 1819-1823.	3.3	8
173	The geomagnetic coast effect in the Pacific Northwest of North America. Geophysical Research Letters, 1985, 12, 502-505.	4.0	11
174	The Long Valley/Mono Basin Volcanic Complex: A preliminary magnetotelluric and magnetic variation interpretation. Journal of Geophysical Research, 1984, 89, 8325-8337.	3.3	29